Self-limiting temperature window for thermal atomic layer etch of HfO_2 and ZrO_2 from the atomic scale mechanism

Rita Mullins,[†,‡] Suresh Kondati Natarajan,[†,¶,‡] Simon D. Elliott,[§] and Michael Nolan[*,†]

†*University College Cork, Tyndall National Institute, Lee Maltings, Dyke Parade, Cork, T12 R5CP, Ireland.*

‡*Authors contributed equally to the manuscript.*

¶*Department of Electrical Engineering and Automation, Aalto University, Espoo 02150, Finland*

§*Schrödinger Inc., 120 West 45 th Street, 17 th Floor, New York, NY 10036-4041, USA.*

E-mail: michael.nolan@tyndall.ie

Abstract

HfO_2 and ZrO_2 are two high-k materials that are important in the down-scaling of semiconductor devices. Atomic level control of material processing is required for fabrication of thin films of these materials at nanoscale device sizes. Thermal Atomic Layer Etch (ALE) of metal oxides, in which up to one monolayer of the material can be removed, can be achieved by sequential self-limiting fluorination and ligand-exchange reactions at elevated temperatures. However, to date a detailed atomistic understanding of the mechanism of thermal ALE of these technologically important oxides is lacking. In this paper, we investigate the hydrogen fluoride pulse in the first step in the thermal ALE process of HfO_2 and ZrO_2 using first principles simulations.

We introduce Natarajan-Elliott analysis, a thermodynamic methodology, to compare reaction models representing the self-limiting (SL) and continuous spontaneous etch (SE) processes taking place during an ALE pulse. Applying this method to the first HF pulse on HfO_2 and ZrO_2 we found that thermodynamic barriers impeding continuous etch are present at ALE relevant temperatures. We performed explicit HF adsorption calculations on the oxide surfaces to understand the mechanistic details of the HF pulse. A HF molecule adsorbs dissociatively on both oxides by forming metal-F and O-H bonds. HF coverages ranging from 1.0 ± 0.3 to 17.0 ± 0.3 HF/nm^2 are investigated and a mixture of molecularly and dissociatively adsorbed HF molecules is present at higher coverages. Theoretical etch rates of -0.61 ± 0.02 Å /cycle for HfO_2 and -0.57 ± 0.02 Å /cycle ZrO_2 were calculated using maximum coverages of 7.0 ± 0.3 and 6.5 ± 0.3 M-F bonds/nm^2 respectively (M = Hf, Zr).

Introduction

The scaling of semiconductor devices means that features are required at the nm scale. As a result of the shrinking of device feature sizes, SiO_2 gate dielectrics would be so thin that electron tunneling through the dielectric layer, which leads to high leakage currents,[1] is impossible to avoid. Materials with high dielectric constant, k, allow a high drive current to be maintained, while minimizing leakage current and a low equivalent oxide thickness can be achieved.[1] HfO_2 and ZrO_2 are high-k dielectric materials with dielectric constants of 22-23,[1,2] which are used in semiconductor devices. HfO_2 and ZrO_2 are also thermodynamically stable when interfaced to silicon in semiconductor applications.[3] However, conformal nm scale feature sizes in high aspect ratio structures are difficult to achieve with traditional wet and dry chemical etch methods which do not permit the level of control required. Recently, atomic layer etching (ALE) has gained significant interest for the controlled etching of thin films, in particular for nanoelectronic devices. ALE shares many features with atomic layer deposition (ALD) and can be considered as the reverse of ALD. ALE permits the removal of

thin films with atomic scale precision using sequential and self-limiting surface reactions,[4–9] similar to ALD.

Traditional ALE processes are anisotropic as they use directional high energy ion bombardment to remove the modified surface layer.[6] Thermal ALE relies on temperature and thermochemically favourable reactions to remove surface species.[10] While there have been many examples of thermal ALE of a range of materials, including: HfO_2,[4,9,11,12] ZrO_2,[4,12] SiO_2,[13] , Al_2O_3,[12,14–18] AlN,[19] AlF_3,[20] TiO_2,[21] TiN,[22,23] W,[24,25] WO_3,[25] ZnO[26] and GaN[27] and for other ALE techniques including Ar neutral beam ZrO_2,[28] plasma ALE SiO_2,[29,30] ZnO,[31] GaN[32,33] and ALE of Si_3N_4[34] using infrared annealing, the details of the mechanism of the ALE process still require significant work to understand.

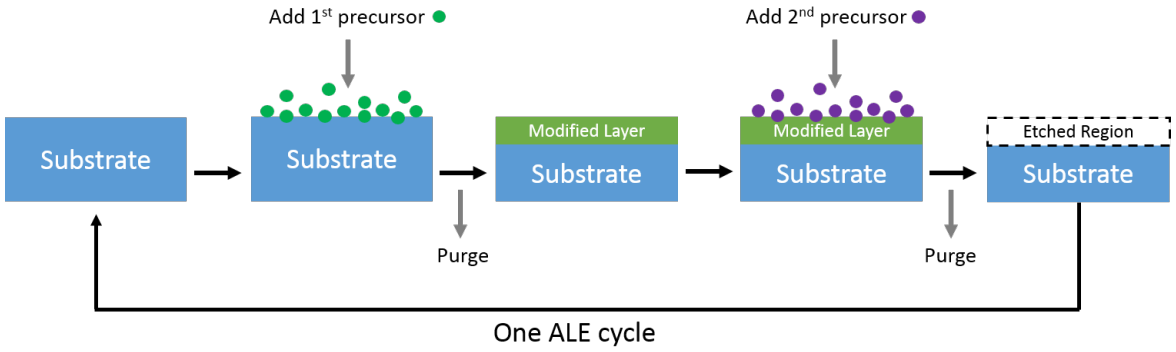

Figure 1: Schematic model of the thermal ALE process.

The first step in ALE is the formation of a reactive but non-volatile layer on the initial film, which is followed by a material removal step to take off only the modified layer as indicated schematically in Figure 1. The key aspect of the ALE process is the self-limiting modification of the pristine film with the first precursor to produce a thin non-volatile surface layer. The purpose of this modification step is to form a reactive, but non-volatile, layer that can be easily removed in the subsequent ligand exchange step.[6,35] To date, reactions during thermal ALE are based on gas-phase fluorination that converts the metal containing film to a layer of the corresponding non-volatile metal fluoride.[4,7,11] For metal oxides, thermal ALE processes generally use HF for the fluorination step.[22] HF is a useful nucleophilic fluorination reactant

where the fluoride anion serves as the active reaction species.[36] This modification step in thermal ALE is the focus of the present paper.

The other half of the thermal ALE cycle consists of a ligand exchange between a metal precursor and the newly formed fluoride layer at elevated temperatures,[4,7,11] for which examples include $Sn(acac)_2$,[4] $Al(CH_3)_3$,[4,37] $Al(CH_3)_2Cl$,[4] $SiCl_4$,[4] $TiCl_4$,[11] BCl_3[21] and WF_6.[24] This second reaction produces stable etch products which are now volatile[36] and can be easily removed, leaving behind a film from which one layer or a fraction of a layer has been removed as shown schematically in Figure 1. Repeating this cycle results in controlled removal of layers from the original film. Other applications of thermal ALE include surface cleaning for the removal of metal impurities in semiconductor fabrication, conformal etching in high aspect ratio structures and smoothing of surfaces to obtain flat and damage free layers which are also important in the semiconductor industry.[7,38] Therefore, thermal ALE is a strong candidate as a processing technology in current and future semiconductor device fabrication.[37]

Given that it is difficult to investigate the ALE reactions directly using experimental techniques, first principles based atomic level simulations using density functional theory (DFT) can give deep insights into the precursor chemistry and the reactions that drive the etch of metal oxides. In this paper, the hydrogen fluoride pulse in the first step in thermal ALE of HfO_2 and ZrO_2 using DFT calculations will be examined. HF molecules adsorb at the surfaces of metal oxides by forming metal-F bonds and there can also be hydrogen bonds between HF molecules. In addition, adsorbed HF may remain intact or dissociate. In the latter case, Hf-F/Zr-F and O-H are formed on HfO_2 and ZrO_2, similar to recent work on Al_2O_3 etch modelling.[39] The amount etched (etch rate) is determined by how much of the oxide surface is fluorinated and how much of the metal fluoride can be removed in the ligand exchange for one ALE cycle.[4]

In addition to investigating HF adsorption, we introduce Natarajan-Elliott analysis (N-E analysis in short), to predict the conditions at which a self-limiting (SL) or continuous

spontaneous etch (SE) reaction becomes thermodynamically favourable, subject to kinetic barriers. This information is useful for directing experimental studies of thermal ALE. Self-limiting reactions are a necessary part of thermal ALE and allow the degree of etching to be well controlled and defined. We find that SL reactions are more favourable than the competing SE reactions for the HF pulse on HfO_2 and ZrO_2 at 0 Kelvin. The temperature above which spontaneous etching is favoured is 657 K and 534 K for HfO_2 and ZrO_2, at typical thermal ALE reactant pressures. Introducing one HF molecule to the bare surfaces of HfO_2 and ZrO_2 results in dissociative adsorption irrespective of the binding site. We determine the maximum coverage of metal-F bonds on the surface and use this coverage to calculate a theoretical etch rate. We also determine the maximum etch rate computed from the lattice constants of HfO_2 and ZrO_2 for one monolayer removal of Hf/Zr. We compare this maximum etch rate to experimental etch rates to calculated the number of Hf/Zr removed per surface area. We study the spontaneous formation of water that resulted from some of our relaxed geometries. This combined thermodynamic and mechanistic investigation using first principles simulation allows us to understand and design novel ALE processes for other technologically relevant materials. We first present a thermodynamic analysis that shows the fluorinated surface is preferred over the oxygen fluoride and then present a detailed analysis of the adsorption coverage of HF molelcules at HfO_2 and ZrO_2 which allows us to also predict etch rates and number of metal atoms removed in a cycle.

Computational Methods

All reported surface slab calculations in this paper are performed using spin-polarized density functional theory as implemented in the VASP[40] 5.4 package. The calculations are based on the generalized gradient approximation (GGA) using the Perdew-Burke-Ernzerhof (PBE) exchange-correlation (XC) functional.[41] The self consistent energy for the electronic minimization is converged within $1x10^{-4}$ eV and the forces for ionic relaxation are converged

within -2x10^{-2} eV/Å. The default smearing method of Methfessel-Paxton 1st order is used with 0.1 eV broadening for electronic relaxation. The core electrons are described by projector augmented wave (PAW) potentials[42] and the valence electrons (Hf: $6s^2$ $5d^2$, Zr: $5s^2$ $4d^2$, O: $2s^2$ $2p^4$, F: $2s^2$ $2p^5$ and H: $1s^1$) are treated using plane wave basis sets with a kinetic energy cut-off of 400 eV. For configurations 2HF B for HfO_2 and ZrO_2 we include the tag IVDW=20 Tkatchenko - Scheffler scheme in our INCAR. We found that their adsorption energies were only increased by ≈ 0.05 eV by including this dispersion method and therefore we do not include it in the below analysis.

Relating SL and SE processes: N-E analysis

The relationship between SE and SL processes of a substrate exposed to a single gaseous reactant is described schematically in Figure 2. In an SL reaction, represented by the solid

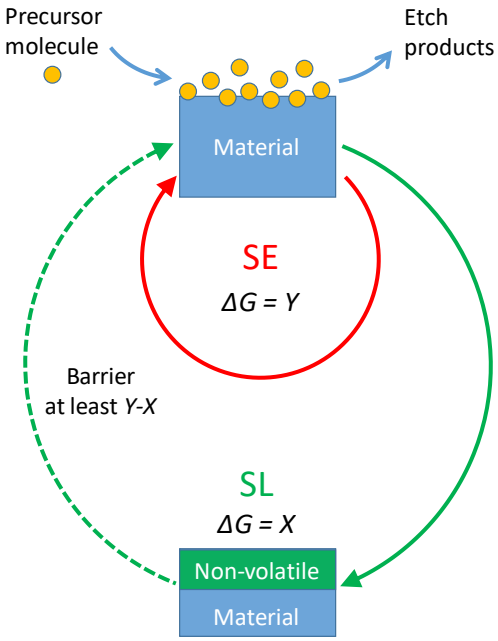

Figure 2: A schematic representation of the relationship between continuous spontaneous etch (SE, red) and self-limiting (SL, green) processes. ΔG represents the reaction free energy.

green arrow in Figure 2, the reactant molecules passivate the material surface and form a non-volatile layer that resists further reaction. Such a reaction is referred to as a "surf →

surf" reaction,

$$\mathrm{SL} : \mathrm{A_{surf}} + \mathrm{B_{gas}} \longrightarrow \mathrm{C_{surf}} \tag{1}$$

with a reaction free energy defined as $\Delta G = X$. Here, the starting surface A is necessarily different from the final surface C. It is possible that by-products are released into the gas phase during this reaction

$$\mathrm{SL} : \mathrm{A_{surf}} + \mathrm{B_{gas}} \longrightarrow \mathrm{C_{surf}} + \mathrm{D_{gas}}. \tag{2}$$

Conversely, in a SE reaction (represented by the solid red arrow in Figure 2) the reactant molecules etch away units of bulk material continuously by forming stable and volatile etch by-products. This continues until the supply of the reactant gas molecules is stopped or the substrate material is exhausted (e.g. an etch stop is reached). Such a reaction is referred to as a "bulk $\longrightarrow$ gas" reaction

$$\mathrm{SE} : \mathrm{A_{surf}} + \mathrm{A_{bulk}} + \mathrm{B_{gas}} \longrightarrow \mathrm{A_{surf}} + \mathrm{E_{gas}} \tag{3}$$

$$\mathrm{SE} : \mathrm{A_{bulk}} + \mathrm{B_{gas}} \longrightarrow \mathrm{E_{gas}} \tag{4}$$

with a reaction free energy $\Delta G = Y$. Clearly, Y is independent of $\mathrm{A_{surf}}$.

The reaction free energy ΔG at temperature T is computed as

$$\Delta G = \Delta H - T\Delta S + RT\ln(Q) \tag{5}$$

$$\Delta H = \Delta E + \Delta\mathrm{ZPE} + \Delta W(T) \tag{6}$$

$$\Delta E = \sum_{\mathrm{p}} \mu E_{\mathrm{p}} - \sum_{\mathrm{r}} \mu E_{\mathrm{r}} \tag{7}$$

$$Q = \prod p^{\mu}_{\mathrm{products}} / \prod p^{\mu}_{\mathrm{reactants}}. \tag{8}$$

In Eq. 5, ΔH and ΔS represent the changes in reaction enthalpy and reaction entropy, respectively. Since the partial pressures of the reactants and products are variable in the

reaction chamber, the $RT\ln(Q)$ term is included. ΔH in Eq. 6 includes three contributions namely, electronic reaction energy ΔE, zero point energy change ΔZPE and a temperature dependent enthalpic contribution $\Delta W(T)$. While the reaction energy (ΔE) in Eq. 7 only includes the bonding information at temperature T=0 K, the reaction free energy (ΔG) provides finite temperature and pressure behaviour of a particular reaction. In Eq. 7, μ refers to the stoichiometric coefficient of the corresponding species and indices r and p indicate reactant and product species, respectively. The reaction quotient Q includes partial pressures of the gas phase reactant and product molecules only. If the reactant and product pressures are the same, then ln$Q$ becomes 0. A negative ΔS increases the free energy and tends to make the reaction more endergonic. Via the translational entropy, the value of ΔS is strongly dependent on the difference in molecularity between the products and the reactants. For example, if the number of gaseous molecules in the products is considerably smaller than in the reactants, then the ΔS value is likely to be negative and to result in an increase of the reaction free energy. In this work we also evaluate the contribution from changes in surface entropy.

A negative value of ΔG means that the corresponding reaction is exergonic (favourable); otherwise it is endergonic (unfavourable). The ΔG values are based on the SE and SL reactions as thermochemically isolated processes. However we find it useful to consider also the overall energetics of the reaction pathway that theoretically links SL to SE (green dotted line in Figure 2). It may be possible to form SE reaction products from the SL reaction products by overcoming one or several energetic barriers. While it is possible to compute kinetic barriers at the first principles level, we omit this in favour of developing a computational approach that allows rapid screening. Balancing the energies in Figure 2 shows that these unknown barriers must be of magnitude at least $Y-X$ (free energy difference of SL and SE reactions) in energy units. This term $Y - X$ will be referred as the "minimum barrier" in this paper.

Based on the values of X and Y we can distinguish the four possible scenarios for the

precursor pulse shown in Figure 3. Each profile in Figure 3 depicts a set of SL and SE

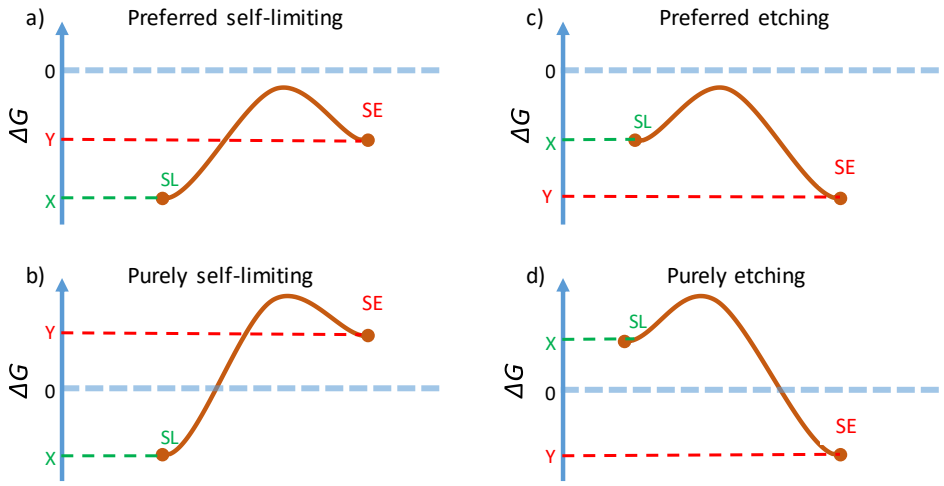

Figure 3: Schematic energy profiles representing a) preferred self-limiting, b) purely self-limiting, c) preferred etching and d) purely etching.

reaction free energies separated by unknown energetic barriers, which in reality may consist of very many barriers in the configurational space of the system. Computing all the reaction pathways and barriers separating the SL and SE product states would be computationally demanding. The aim of this methodology is to form useful conclusions without computing these pathways, thus accelerating process design. The minimum possible barrier to drive the etch reaction from the SL to SE product state is $Y - X$ in energy units as mentioned earlier. In the energy profiles, the SL reaction appears on the left hand side of the horizontal axis since the precursor molecules must first react with the surface before accessing the bulk. In order to cause etching from there onward, the precursor molecules may have to lift the surface atoms out of their lattice positions or diffuse into the sub-surface region, and finally form volatile products. Therefore the SE reaction is shown to the right of the SL reaction in these energy profiles.

Depending on whether the SL reaction or the SE reaction is the most favourable (based on their ΔG values) the energy profiles in Figure 3 are classified broadly as self-limiting or etching. The energy profile in Figure 3a is termed as 'preferred self-limiting' since the SL reaction is more thermodynamically favoured than the SE reaction even though both

SL and SE reactions are exergonic. Here, there is a possibility of etching if the collective barrier (at least $Y - X$) could be overcome under the reactor conditions. If the energy profile in Figure 3a is shifted along the vertical axis such that the SL reaction is exoergic and the SE reaction is endergonic, we obtain the energy profile in Figure 3b termed as 'purely self-limiting'. This is the ideal energy profile for the surface modification pulse in an ALE process since unlimited etching is energetically unfavourable. The energy profile in Figure 3c is the reverse of that in Figure 3a since the SE reaction is energetically more favourable than the SL reaction ($Y - X < 0$). The collective barrier, if any, for etching would be comparatively lower than in the 'preferred self-limiting' state and it may be easily breached under the reactor conditions. Therefore, the energy profile in Figure 3c is termed as 'preferred etching'. Figure 3d is obtained by shifting the energy profile in Figure 3c such that the SL reaction is endergonic and the SE reaction is exergonic. This profile is termed as 'purely etching' since the precursor molecules should readily volatilize the surface atoms and proceed to the sub-surface region to cause bulk etching without significant barriers. This is the ideal energy profile for a SE pulse. Thus, the shape of the energy profile at any given temperature and pressure will allow us to predict the net effect of the precursor-substrate interaction. We refer to this computational approach as the N-E analysis.

To summarise, by comparing the energetics and thermodynamics of the SE (bulk $\longrightarrow$ gas) and SL (surf $\longrightarrow$ surf) reactions, along with the minimum energetic barrier separating them, we can predict whether the gas of a particular precursor pulse will spontaneously etch the substrate material at the temperatures and pressures of interest.

Bulk and Slab Models

We have optimized the bulk unit cell of monoclinic HfO_2 (space group: $P2_1/c$) and ZrO_2 (space group: $P2_1/c$) by simultaneously relaxing the ionic positions, cell shape and cell volume with an energy cutoff of 550 eV and a Monkhorst-Pack K-point sampling mesh of (6 x 6 x 6). The bulk monoclinic unit cells of HfO_2 and ZrO_2 have 4 metal atoms and 8 O

atoms. The optimized lattice constants of HfO_2 from this set-up are: a = 5.142 Å, b = 5.195 Å and c = 5.326 Å, while the lattice constants of ZrO_2 are: a = 5.140 Å, b = 5.189 Å and c = 5.239 Å. Comparing our values to the experimental values for the baddeleyite phase,[43] the deviations for HfO_2 are: a = 0.43 %, b = 0.48 % and c = 0.96 % and for ZrO_2: a = 0.58 %, b = 0.78 % and c = 1.89 %.

A surface slab of monoclinic HfO_2 and ZrO_2 with a (111) orientation is used for the surface calculations as this is the most stable facet at low temperatures and has the lowest surface energy.[43,44] A surface supercell of HfO_2 and ZrO_2 with a (2 x 2) expansion of the hexagonal unit cell and 16 Å of vacuum separating the slabs is used for the surface models; this has a stoichiometry of $Hf_{80}/Zr_{80}O_{160}$ per supercell. It consists of 5 layers of 16 HfO_2/ZrO_2 units and a k-point sampling mesh of (2x2x1) is used for geometry optimization. The product states of the SL reactions needed for the N-E analysis are obtained by adding 2 F atoms per surface O removed (for brevity we denote this ratio as 1O:2F) from the top layer of the slab models. We consider three product states for our analysis: 8O:16F, 12O:24F and 16O:32F. For the surface slabs, enthalpy H and entropy S are computed using the Phonopy code by considering only the first layer of atoms.[45] The calculations for the reactant molecules and gas phase by-products are performed in VASP with a large periodic box of dimensions 15.0 Å x 16.0 Å x 15.5 Å and 400 eV plane wave energy cutoff. The enthalpy and entropy for the gas phase molecules were calculated from the freeh program in the Turbomole suite[46] at 1 atm pressure. The above calculations are performed with the PBE exchange-correlation functional[41] and a polarized triple zeta basis set (def-TZVPP)[47,48] and default medium grid.

For the HF adsorption studies, the molecules are introduced at various surface sites and at different coverages on the (111) surface slabs of HfO_2 and ZrO_2. The absorbate coverages and binding energies are computed and a surface model with maximum coverage of metal-F is then used to derive the theoretical etch rate for the HF pulse on HfO_2 and ZrO_2.

The VASP data can be found at the GitHub repository `https://github.com/RitaMull/Thermal-ALE-HfO2-and-ZrO2-with-HF`

Results

In the first part of this section, we will perform the N-E analysis and compare self-limiting with spontaneous etch reaction models. In the next part, the adsorption mechanism of HF at a range of coverages on HfO_2 and ZrO_2 will be studied, together with analysis of H_2O formation. Finally, a theoretical etch rate is predicted based on the maximum possible coverage of dissociated HF on the material surfaces.

Self-Limiting Vs Spontaneous Etch

Comparing the energetics and thermodynamics of the SL and SE model reactions for the fluorination of HfO_2 and ZrO_2 using HF, we can predict if the HF pulse will spontaneously etch or result in a self-limiting reaction at the given conditions. Model reactions representing the HF pulse on HfO_2 and ZrO_2 are listed in Table 1 together with the corresponding reaction (free) energies at 0 K and 500 K, with a reactant pressure of 0.2 Torr and a product pressure of 0.01 Torr, as computed from DFT calculations.

	Reactions	ΔE [eV/M]	ΔG [eV/M]
	HfO_2		
SE1	1 $HfO_{2(b)}$ + 4 $HF_{(g)}$ → 1 $HfF_{4(g)}$ + 2 $H_2O_{(g)}$	-0.91	-0.65
SL1	1 $HfO_{2(surf)}$ + 4 $HF_{(g)}$ → 1 $HfF_{4(surf)}$ + 2 $H_2O_{(g)}$	-3.27 (2.36)	-1.20 (0.55)
SE2	1 $HfO_{2(b)}$ + 2 $HF_{(g)}$ → 1 $HfOF_{2(g)}$ + 1 $H_2O_{(g)}$	3.87	3.10
SL2	1 $HfO_{2(surf)}$ + 2 $HF_{(g)}$ → 1 $HfOF_{2(surf)}$ + 1 $H_2O_{(g)}$	-1.64 (5.51)	-0.60 (3.70)
	ZrO_2		
SE1	1 $ZrO_{2(b)}$ + 4 $HF_{(g)}$ → 1 $ZrF_{4(g)}$ + 2 $H_2O_{(g)}$	-1.14	-0.89
SL1	1 $ZrO_{2(surf)}$ + 4 $HF_{(g)}$ → 1 $ZrF_{4(surf)}$ + 2 $H_2O_{(g)}$	-3.04 (1.90)	-1.00 (0.11)
SE2	1 $ZrO_{2(b)}$ + 2 $HF_{(g)}$ → 1 $ZrOF_{2(g)}$ + 1 $H_2O_{(g)}$	2.96	2.19
SL2	1 $ZrO_{2(surf)}$ + 2 $HF_{(g)}$ → 1 $ZrOF_{2(surf)}$ + 1 $H_2O_{(g)}$	-1.52 (4.48)	-0.50 (2.69)

Table 1: Reaction energies ΔE at 0 K and reaction free energies ΔG at 500 K of the model SE and SL reactions representing the HF pulse on HfO_2 and ZrO_2. The value within parenthesis corresponds to the minimum barrier between the respective SE and SL reactions. The product state of SL1 and SL2 reactions is the 8O:16F surface of MO_2 (M = Hf/Zr) as described in the previous section and the reaction energy is listed per modified M atom.

This table also includes the minimum barrier to cause spontaneous etch as already discussed. Negative minimum barriers indicate that spontaneous etch is thermodynamically favourable and is hindered only by kinetic barriers, if any. Two SE reactions and two SL reactions are postulated for HF exposure on both HfO_2 and ZrO_2. The SE reactions involve the complete conversion of the bulk metal oxide to volatile metal fluoride (SE1) or metal oxyfluoride (SE2) and water, while the corresponding SL reactions involve conversion of the outermost surface layer of the metal oxide to the non-volatile metal (oxy)fluoride (terminating the metal oxide), releasing water molecules. For the SE1 reaction of Hf/ZrO_2 4 HF molecules are needed to etch away one unit of bulk Hf/ZrO_2 to form Hf/ZrF_4 and H_2O. For the SE2 reaction for Hf/ZrO_2, 2 HF molecules are required to etch a unit of Hf/ZrO_2 to form Hf/$ZrOF_2$ and H_2O. In the SE reactions, the surface of the material before and after each precursor pulse will be identical and therefore their contributions are ignored from the reaction model. For the SL reactions the surfaces are not identical before and after the pulse and their contributions have to be included. In Table 1, the SL product state of the surfaces is 8O:16F (refer ESI for the geometry).

A negative reaction (free) energy (ΔG) means the reaction is exergonic (favourable) and a positive ΔG is endergonic (unfavourable). The SE2 reactions forming volatile metal oxyfluorides are unfavorable at 0 K and 500 K as the reaction (free) energy is positive (unfavourable), whereas the SE1 reactions forming volatile metal fluorides are favourable. For all the SL-SE combinations at 0 K, for both materials, the minimum barrier to etch was positive suggesting that self-limiting reaction is the most favourable energetically. At 500 K, the thermodynamic barrier is reduced considerably which means high temperatures favour SE reactions. In any case, below 500 K, the minimum barrier is positive suggesting that SL reactions are preferred for both metal oxides. Therefore, up to 500 K, the reactions are in

'preferred self-limiting' state for both materials. Therefore we can propose that the reaction of HF in the first step will self-limit on both metal oxides at least up to 500 K.

As the SE1 reactions forming the volatile metal fluoride are more favourable than the SE2 reactions that form the oxyfluoride, we will consider only the SE1 reactions for further analysis. Moreover, the barrier to etch was very high for the SL2-SE2 reactions as compared to the SL1-SE1, even at 500 K, suggesting that spontaneous formation of oxy-fluoride is not probable at ALE relevant temperatures.

Reaction Free Energy Profiles

The free energy profiles (FEPs) of the reactions in Table 1 are discussed in this section. Comparing the reaction free energy profiles (FEPs) of the SE and SL reactions, we can determine at a given temperature and reactant pressure whether the HF pulse will favour spontaneous etching or self-limited conversion of HfO_2 and ZrO_2 to a non-volatile metal fluoride layer. Here we use a reactant pressure of 0.2 Torr and a product pressure of 0.01 Torr within a temperature range of 0-1000 K. The various contributions to the free energy for the example of the SE1 reaction for HfO_2 are plotted in Figure 4.

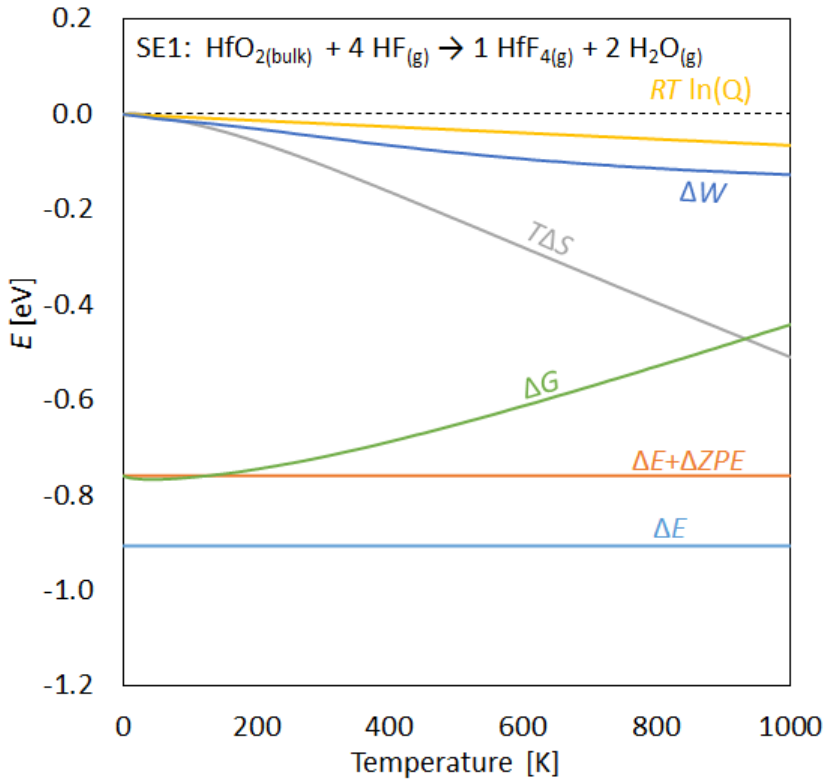

Figure 4: Contributions to the reaction FEP of the SE1 reaction of HfO_2 shown in Table 1. RTln(Q) in gold accounts for the partial pressures of the reactants and products, enthalpic contribution (ΔW) is given in dark blue , entropy term (TΔS) in grey , reaction energy (ΔE) in light blue, sum of reaction energy and zero point energy change (ΔE + ΔZPE) in brown and reaction free energy (ΔG) in green.

In Figure 4, the ΔE and ΔZPE contributions are temperature independent. TΔS is the entropy contribution and is 0 eV at 0 K and -0.5 eV at 1000 K. The entropy term decreases with increasing temperature because four gaseous reactant molecules result in the formation of three product molecules only. The *RTln(Q)* and ΔW contributions are clearly smaller by comparison to the entropy term. They decrease the free energy at high temperatures and compete against the entropy term that increases the free energy with temperature. The FEP of this reaction at the reactant and product pressures stated above is exergonic up to 1000 K. The other reactions show similar contributions.

The FEPs of the SE1 and SL1 reactions of HfO_2 and ZrO_2 are compared in Figure 5. For HfO_2, the self-limiting reaction is preferred up to 656 K. At 657 K the SE1 and SL1 reactions are isoenergetic with the minimum barrier becoming zero and beyond this the SE1 reaction

is more favourable. Finally, at 813 K the self-limiting reaction becomes endergonic and continuous etching dominates. We see similar trends for ZrO_2, with self-limiting reactions preferred up to 533 K, while at 770 K the self-limiting reaction becomes endergonic and continuous etching remains exergonic.

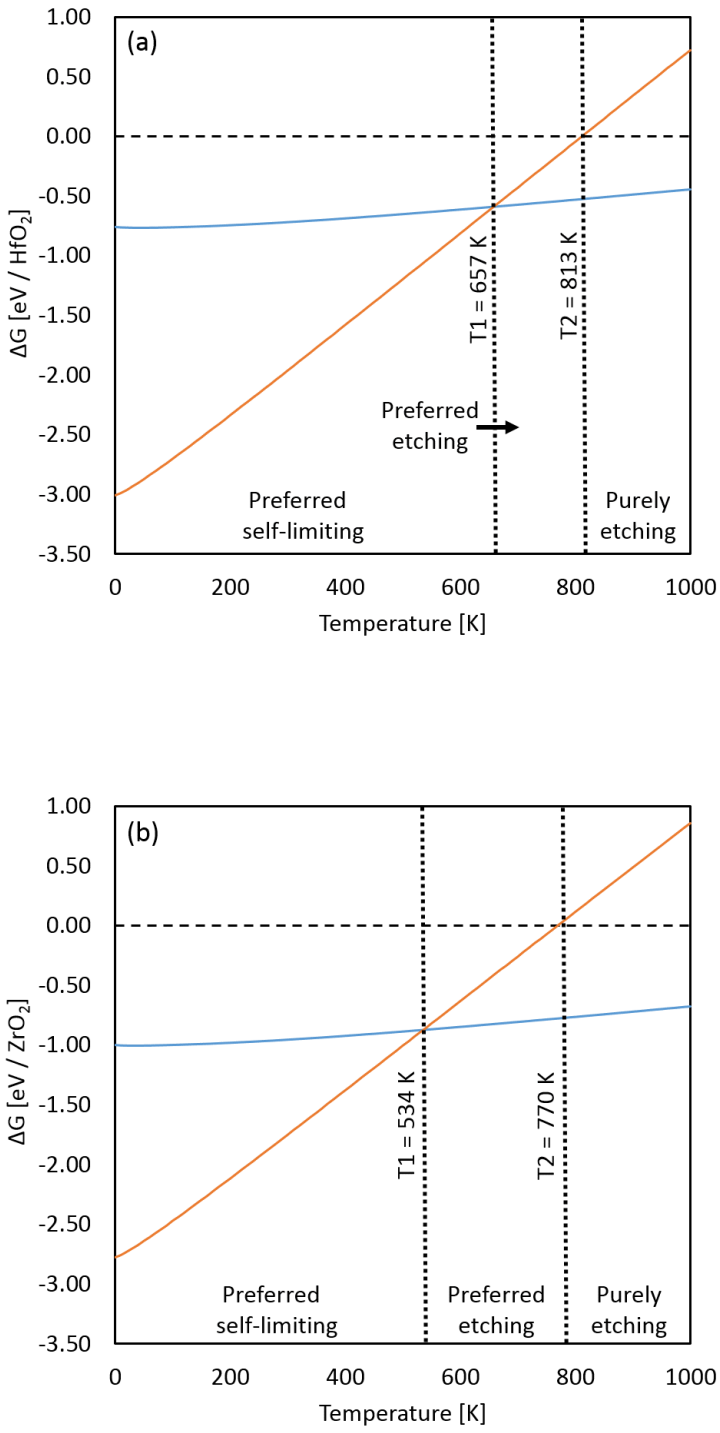

Figure 5: Free energy profiles for the SE1 (blue) and SL1 (orange) reactions of HfO_2 (a) and ZrO_2 (b) from 0 to 1000 K at the pressures given in the text. T1 is where the self-limiting and spontaneous etch reactions cross over for the 8O:16F model and T2 is where spontaneous etching is preferred.

In Figure 5, the FEP is computed using 8O:16F model as the SL product state. For completeness, we also determine the FEPs for two other SL product models, namely 12O:24F and 16O:32F. Both surfaces of HfO_2 and ZrO_2 have 16 topmost O atoms (oxygen) in the supercell that could react with the HF molecules. For the 12O:24F product state, $\frac{3}{4}$ of surface O are removed and 24 F (fluorine) are added to replace them. For the 16O:32F, all surface O are removed and 32 F are added to replace them. All oxygen atoms were removed as H_2O molecules. Basically, the M-O (M = Hf, Zr) coordination numbers of the surface metal atoms are decreasing from 8O:16F to 16O:32F. Note that the more O atoms are removed, the easier it would be to remove the surface metal atoms in the second pulse due to the reduced metal-O interaction. Therefore we use the 12O:24F and 16O:32F product states merely as extreme test cases to compare their thermodynamic stability with the more reasonable 8O:16F model. The geometries used for the SL thermochemical calculations of both metal oxides are shown in section S1 of the Supporting Information. Table 2 shows the energetics for the SL reactions including 12O:24F and 16O:32F models.

	SL product state	ΔE [0 K] [eV/M]	ΔG [500 K] [eV/M]
	HfO_2		
SE1	HfF_4	-0.91	-0.65
SL1	8O:16F	-3.27 (2.36)	-1.20 (0.55)
SL2	12O:24F	-3.05 (2.14)	-1.04 (0.39)
SL3	16O:32F	-2.45 (1.54)	-0.41 (-0.24)
	ZrO_2		
SE1	ZrF_4	-1.14	-0.89
SL1	8O:16F	-3.04 (1.90)	-1.00 (0.11)
SL2	12O:24F	-2.91 (1.77)	-0.90 (0.01)
SL3	16O:32F	-2.17 (1.03)	-0.11 (-0.78)

Table 2: Reaction (free) energies and minimum barriers within parenthesis at 0 K and 500 K for the model SL reactions representing the HF pulse on HfO_2 and ZrO_2 for 8O:16F, 12O:24F and 16O:32F SL product states, (M = Hf, Zr)

.

At 0 K, all SL reactions are more favourable than the SE reaction for both oxides and the minimum barriers are positive. For both oxides, we find the minimum barrier to decrease with the number of surface O atoms removed, with the lowest barriers for ZrO_2. At 500 K, the SL1 and SL2 reactions continue to be more favourable than the SE reaction, whereas, the SL3 reaction is not. This means that an aggressive removal of surface O by HF during the first pulse would also enhance etching of the surface Hf/Zr atoms at ALE relevant temperatures, say 500 K.

Experimental work showed that HF reaction is self-limiting on HfO_2 at 200 °C (473 K),[9] at 250 °C (523 K)[11] and at 300 °C (573 K).[11] Comparing to Figure 6 this is true for partial surface O removal (8O:16F) where self-limiting is preferred up to 618 K for $\frac{3}{4}$ of surface O removal and up to 657 K for $\frac{1}{2}$ of surface O removal. The same analysis holds for ZrO_2. Therefore, N-E analysis is a simple and relatively inexpensive method to predict the structure of the surface after the first ALE pulse. We will further validate this methodology on experimental results for different ALE processes in a future publication.

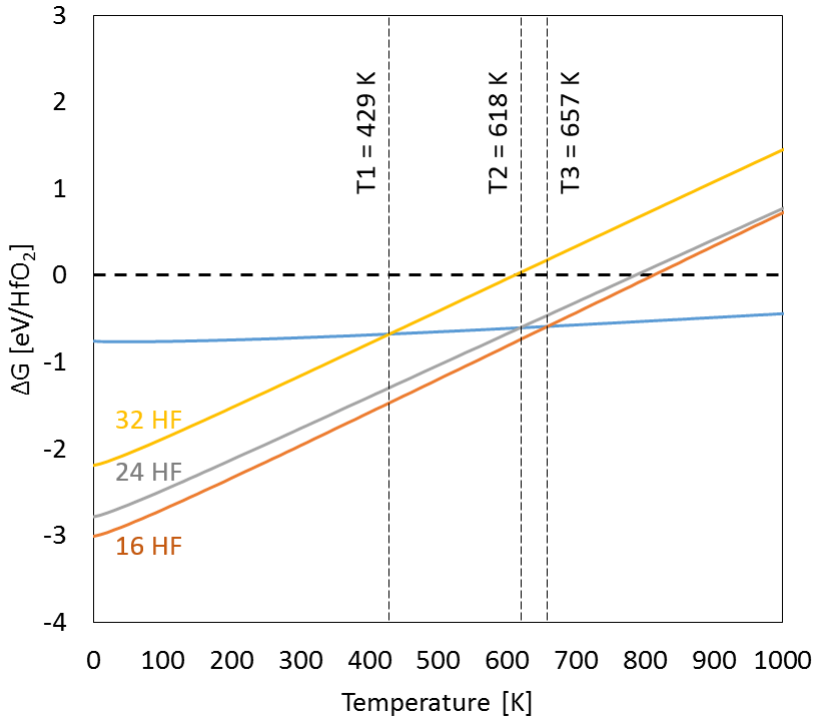

Figure 6: Free Energy Profiles of the continuous etching and self-limiting reactions for HfO_2. T1, T2 and T3 are where the self-limiting and spontaneous etch reactions cross over for 16O:32F, 12O:24F and 8O:16F models respectively.

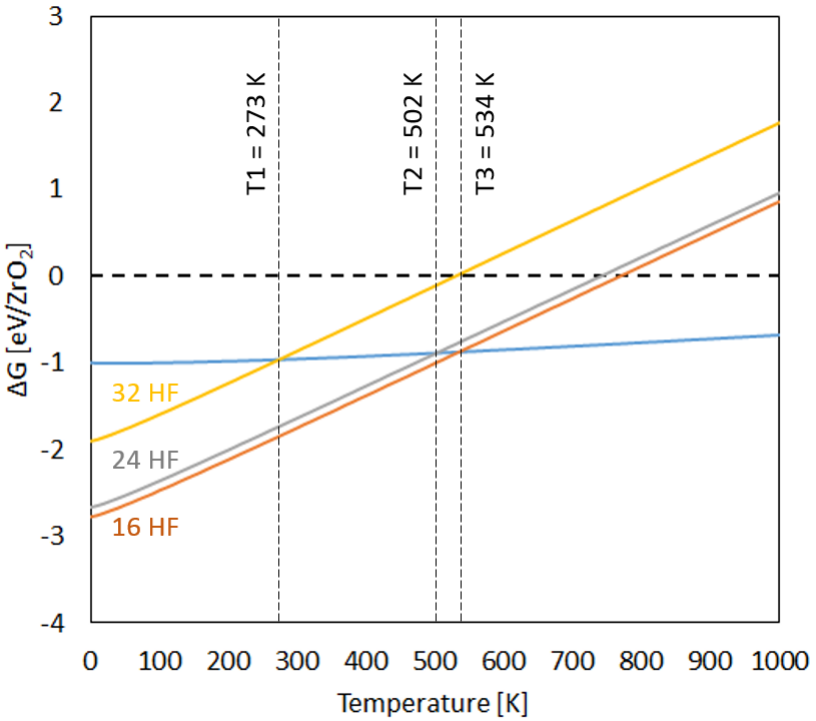

Figure 7: Free Energy Profiles of the continuous etching and self-limiting reactions for ZrO_2. T1, T2 and T3 are where the self-limiting and spontaneous etch reactions cross over for 16O:32F, 12O:24F and 8O:16F models respectively.

Adsorption of 1 HF Molecule at HfO_2 and ZrO_2

Natarajan and Elliott[39] studied the adsorption of HF on the bare surface of Al_2O_3 and found that Al-F bonding is crucial for HF dissociation. To find if the same holds for HfO_2 and ZrO_2, we adsorb one HF molecule to the optimized bare surfaces of both oxides at different binding sites (which we term A, B and C). These sites were chosen to test if molecular or dissociative adsorption of HF is sensitive to the adsorption site. The different binding sites for 1 HF are shown in section S2 of the Supporting Information.

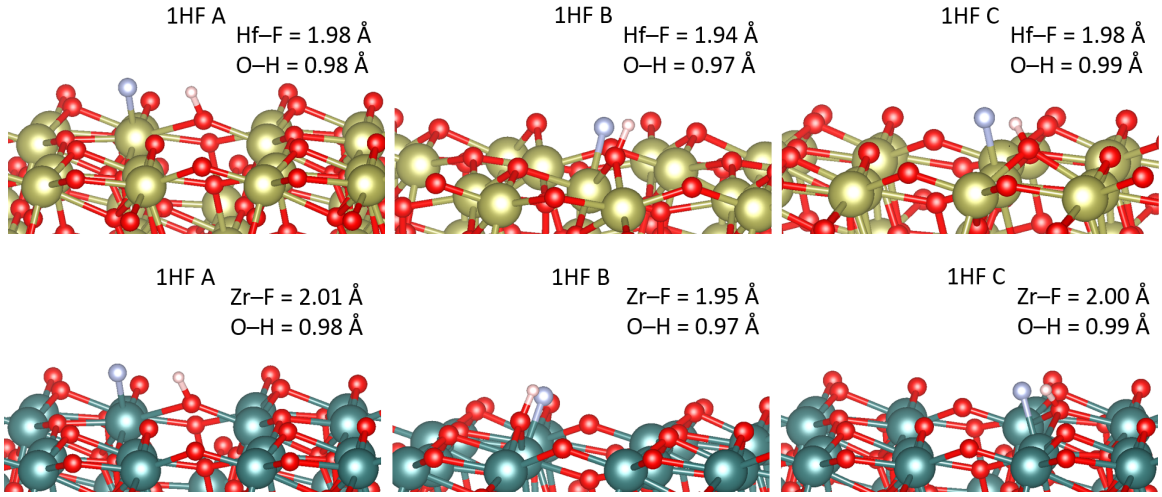

Figure 8: Relaxed adsorption structures for 1 HF molecule interacting with the bare surfaces of HfO_2 and ZrO_2. The colour coding is: yellow = Hf, green = Zr, red = O, white = H and blue = F.

Figure 8 shows that the HF molecule is spontaneously dissociated at each binding site to form metal-F and O-H bonds on both oxides. No molecular HF adsorption was found. Similar to the Al_2O_3 case, we find that the HF dissociation proceeds after a stable M-F (M = Hf, Zr) bond is formed. The computed adsorption energies for the dissociative adsorption of one 1 HF molecule on the bare surface of HfO_2 are: -1.52 eV, -1.95 eV and -1.63 eV at sites A, B and C respectively. The corresponding values for ZrO_2 are: -1.25 eV, -1.74 eV and -1.48 eV.

The interaction between HfO_2 and HF is 0.15 eV to 0.21 eV stronger than between ZrO_2 and HF. The Hf-F, Zr-F and O-H bond lengths are shown for each adsorption mode in Figure 8. The surface O atoms are either 2-fold are 3-fold coordinated by surface Hf/Zr atoms on both surfaces. All the surface Hf/Zr atoms are 6-fold coordinated by O atoms. Since the structures of HfO_2 and ZrO_2 are similar, the strongest adsorption mode (1HF B for HfO_2 -1.95 eV and for ZrO_2 -1.74 eV) involve the same 6-fold coordinated metal lattice site and 2-fold coordinated surface oxygen site.

Stability of different HF Coverages

The stability of different HF coverages was examined by introducing up to 34 randomly oriented HF molecules per supercell ca. 3 Å from the bare monoclinic (111) surface of HfO_2 and ZrO_2; this results in coverages ranging from 1.0 ± 0.3 to 17.0 ± 0.3 HF/nm^2 (2 HF to 34 HF molecules per supercell). There are 16 topmost metal atoms on the surface of the (2x2) supercell that may form metal-F bonds on both oxides. There are also 16 surface oxygen on the bare surface of each metal oxide that can form O-H bonds or, as seen in some simulations, H_2O which we discuss later. For each metal oxide three different configurations (A, B and C) were examined for the range of HF coverages using 2, 3, 4, 5 and 8 molecules per supercell and two configurations (A and B) using 12 and 16 molecules per supercell and one configuration for 30, 32 and 34 molecules per supercell. The computed energies of adsorption for the above mentioned geometries are shown in Tables 3 and 4.

HfO_2	Coverage		E_{bind}	
	adsorbed HF	(Hf-F, dissociated F)		
Geometry	nm^{-2}	nm^{-2}	eV/HF	eV/nm^2
2HF A (2, 2)	**1.0**	**(1.0, 1.0)**	**-1.5**	**-1.5**
2HF B (1, 1)	1.0	(0.5, 0.5)	-0.8	-0.8
2HF C (1, 1)	1.0	(0.5, 0.5)	-1.0	-1.0
3HF A (2, 2)	1.5	(1.0, 1.0)	-1.1	-1.7
3HF B (2, 2)	1.5	(1.0, 1.0)	-1.1	-1.6
3HF C (3, 3)	**1.5**	**(1.5, 1.5)**	**-1.7**	**-2.6**
4HF A (3, 3)	2.0	(1.5, 1.5)	-1.3	-2.6
4HF B (3, 3)	2.0	(1.5, 1.5)	-1.3	-2.7
4HF C (4, 4)	**2.0**	**(2.0, 2.0)**	**-1.6**	**-3.2**
5HF A (5, 5)	**2.5**	**(2.5, 2.5)**	**-1.8**	**-4.6**
5HF B (4, 4)	2.5	(2.0, 2.0)	-1.4	-3.4
5HF C (5, 5)	2.5	(2.5, 2.5)	-1.5	-3.7
8HF A (5, 4)	4.0	(2.5, 2.0)	-1.1	-4.6
8HF B (6, 6)	**4.0**	**(3.0, 3.0)**	**-1.3**	**-5.2**
8HF C (6, 5)	4.0	(3.0, 2.5)	-1.1	-4.4
12HF A (10, 7)	**6.0**	**(5.0, 3.5)**	**-1.3**	**-7.7**
12HF B (10, 7)	6.0	(5.0, 3.5)	-1.2	-7.3
16HF A (12, 8)	8.0	(6.0, 4.0)	-1.1	-9.0
16HF B (13, 9)	**8.0**	**(6.5, 4.5)**	**-1.2**	**-9.6**
30HF (12, 7)	15.0	(6.0, 3.5)	-0.8	-11.8
32HF (12, 6)	16.0	(6.0, 3.0)	-0.8	-12.1
34HF (14, 7)	17.0	(7.0, 3.5)	-0.9	-12.9

Table 3: Adsorbate coverages and binding energies for the HF coverages on HfO_2 surface shown in Figure 9 and in S4 of the Supporting Information. The first number in parenthesis within the first column corresponds to the total number of Hf-F bonds and the second number correspond to the number of dissociated HF molecules. The most stable configurations, when more than one configuration is studied for a coverage, are highlighted in bold.

ZrO_2	Coverage		E_{bind}	
	adsorbed HF	(Zr-F, dissociated F)		
Geometry	nm^{-2}	nm^{-2}	eV/HF	eV/nm^2
2HF A(1, 1)	1.0	(0.5, 0.5)	-0.9	-0.9
2HF B (1, 1)	1.0	(0.5, 0.5)	-1.0	-1.0
2HF C (2, 2)	**1.0**	**(1.0, 1.0)**	**-1.2**	**-1.2**
3HF A (2, 2)	1.5	(1.0, 1.0)	-1.0	-1.6
3HF B (3, 2)	**1.5**	**(1.5, 1.0)**	**-1.2**	**-1.9**
3HF C (2, 2)	1.5	(1.0, 1.0)	-0.8	-1.2
4HF A (4, 4)	2.0	(2.0, 2.0)	-1.4	-2.6
4HF B (4, 4)	**2.0**	**(2.0, 2.0)**	**-1.5**	**-3.1**
4HF C (3, 3)	2.0	(1.5, 1.5)	-1.1	-2.2
5HF A (5, 4)	2.5	(2.5, 2.0)	-1.3	-3.2
5HF B (4, 4)	2.5	(2.0, 2.0)	-1.1	-2.8
5HF C (4, 4)	**2.5**	**(2.0, 2.0)**	**-1.3**	**-3.3**
8HF A (7, 7)	4.0	(3.5, 3.5)	-1.2	-5.0
8HF B (7, 7)	**4.0**	**(3.5, 3.5)**	**-1.3**	**-5.1**
8HF C (7, 7)	4.0	(3.5, 3.5)	-1.2	-4.9
12HF A (9, 6)	6.0	(4.5, 3.0)	-1.0	-6.0
12HF B (9, 7)	**6.0**	**(4.5, 3.5)**	**-1.0**	**-6.3**
16HF A (10, 8)	8.0	(5.0, 4.0)	-1.0	-7.9
16HF B (11, 7)	**8.0**	**(5.5, 3.5)**	**-1.1**	**-8.6**
30HF (13, 8)	15.0	(6.5, 4.0)	-0.8	-11.5
32HF (12, 6)	16.0	(6.0, 3.0)	-0.7	-11.5
34HF (13, 8)	17.0	(6.5, 4.0)	-0.7	-12.3

Table 4: Adsorbate coverages and binding energies for the HF coverages on the ZrO_2 surface shown in Figure 10 and in S4 of the Supporting Information. The first number in parenthesis within the first column corresponds to the total number of Zr-F bonds and the second number correspond to the number of dissociated HF molecules. The most stable configurations, when more than one configuration is studied for a coverage, are highlighted in bold.

For HfO_2, spontaneous complete dissociation of the adsorbed HF molecules was observed for some configurations with coverages of 2, 3, 4 and 5 HF molecules, as shown in Figure 9. Similarly, for ZrO_2, complete dissociation of adsorbed HF was seen for some configurations with coverages of 2 and 4 HF molecules only as shown in Figure 10. However, for the

adsorption of 3, 5 and 8 HF molecules on the ZrO_2 surface, upon relaxation, there were 2, 4 and 7 dissociated HF molecules present for each configuration (A, B or C); see S4 of the Supporting Information.

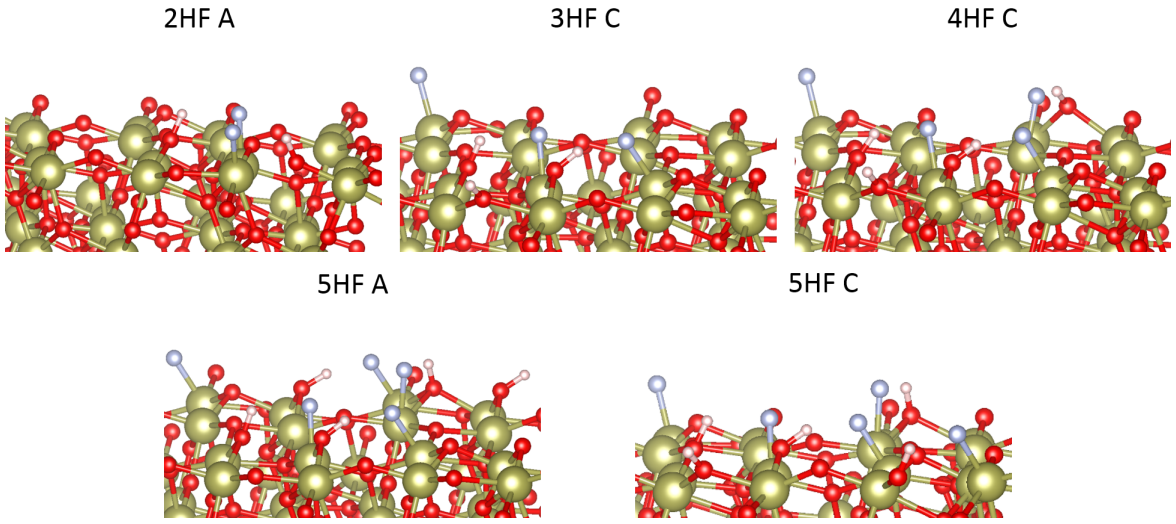

Figure 9: Relaxed geometries for HF coverages 2A, 3C, 4C, 5A and 5C of HfO_2 where complete dissociation of HF occurred spontaneously. Colour coding is the same as figure 8.

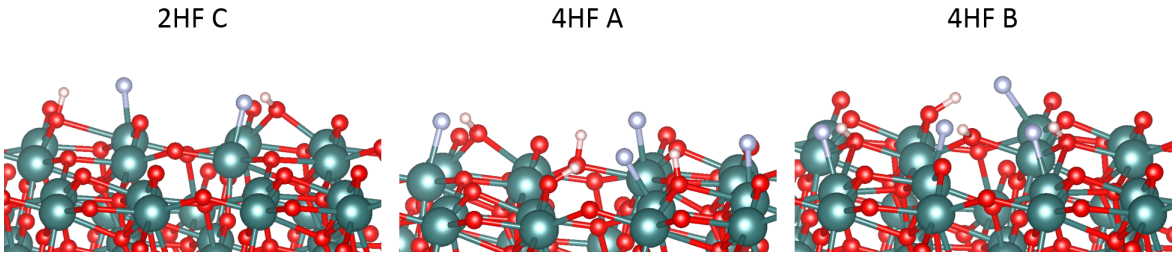

Figure 10: Relaxed geometries for HF coverages 2C, 4A and 4B of ZrO_2 where complete dissociation of HF occurred spontaneously. Colour coding is the same as figure 8.

In all other HF adsorption configurations for HfO_2 and ZrO_2, we find a mixture of molecular and dissociative adsorption of the HF molecules. We have computed binding energies per HF and per unit surface area of the material as listed in Tables 3 and 4.

For both metal oxides the binding energy is more favourable as the extent of metal-F bonding increases on the bare surface. This can be seen for HfO_2 in Table 3 and Figure 11 plot (c) with Hf-F coverage from 1.0 ± 0.3 to 7.0 ± 0.3 nm^{-2} with surface binding energies -1.5 to -12.9 eV/nm^2. Similar trends are also seen for ZrO_2 in Table 4 and Figure 12 plot

(c) with Zr-F coverage from 1.0 ± 0.3 to 6.5 ± 0.3 nm^{-2} with surface binding energies -0.9 to -12.3 eV/nm^2. The HF molecules that did not dissociate in the relaxed geometries shown in S4 of the Supporting Information form hydrogen bonds with the remaining HF molecules and dissociated F atoms. For higher HF coverages, a more extensive hydrogen bonded HF network is expected. There are intact HF molecules forming M-F bonds as well (M = Hf, Zr), whose coverage is found by subtracting the two numbers within parenthesis in Tables 3 and 4. These metal bound HF molecules (M-FH) are not likely to be purged away in the next ALE step as they form strong bonds (Hf-F 6.7 eV and Zr-F 6.5 eV)[49] and these HF molecules should likely dissociate when the kinetic barriers are overcome inside the reactor. Therefore, we will use the total number of M-F bonds for the etch rate prediction in a later section.

Plot (a) in Figures 11 and 12 show scatter plots for metal-F coverage versus adsorbed HF coverage from the data in Tables 3 and 4 for HfO_2 and ZrO_2. The dashed line shows a linear correlation between HF adsorption and metal-F coverage which indicates the cases where all adsorbed HF molecules form metal-F bonds. The square data points along the dashed lines are those geometries where adsorbed HF coverage equals metal-F coverage. For HF adsorption at HfO_2, this corresponds to the most stable configurations at coverages of 1.0, 1.5, 2.0 and 2.5 HF/nm^2. For ZrO_2, this corresponds to the most stable configurations at coverages of 1.0 and 2.0 HF/nm^2. Note that the data points of (2HF B & 2HF C), (3HF A & 3HF B), (4HF A & 4HF B), (5HF A & 5HF C), (8HF B & 8HF C), and (12HF A & 12HF B) overlap in Figure 11 (a) as their adsorbed HF and Hf-F coverages are the same. Similarly, the data points of (2HF A & 2HF B), (3HF A & 3HF C), (4HF A & 4HF B), (5HF B & 5HF C), (8HF A & 8HF B & 8HF C), and (12HF A & 12HF B) overlap in Figure 12 (a). The points at higher HF coverages correspond to those geometries in which partially dissociated HF molecules are present and hence the points lie below the correlation line. As the HF coverage increases the metal-F coverage starts to plateau suggesting maximal coverages of 6.0±0.3 to 7.0±0.3 metal-F/nm^2. Lee et al.[9] found that for low HF coverages

during etch of HfO_2 using HF and $Sn(acac)_2$ there was a lack of self-limiting behaviour as the HF reaction had not reached saturation. We also find from plots (b) and (c) of Figures 11 and 12 that a saturation in the binding energy is not reached even at high HF coverages. Therefore, the highest adsorbed HF coverage of 34 HF with M-F coverage (M = Hf, Zr) of 7.0 ± 0.3 metal-F/nm^2 and 6.5 ± 0.3 metal-F/nm^2 will be used as the maximum coverage for the HfO_2 and ZrO_2 etch rate prediction respectively. We added an exponential fit to the data in plot (b) of Figures 11 and 12 in section 6 of ESI along with its derivative which provides HF addition energy indirectly.

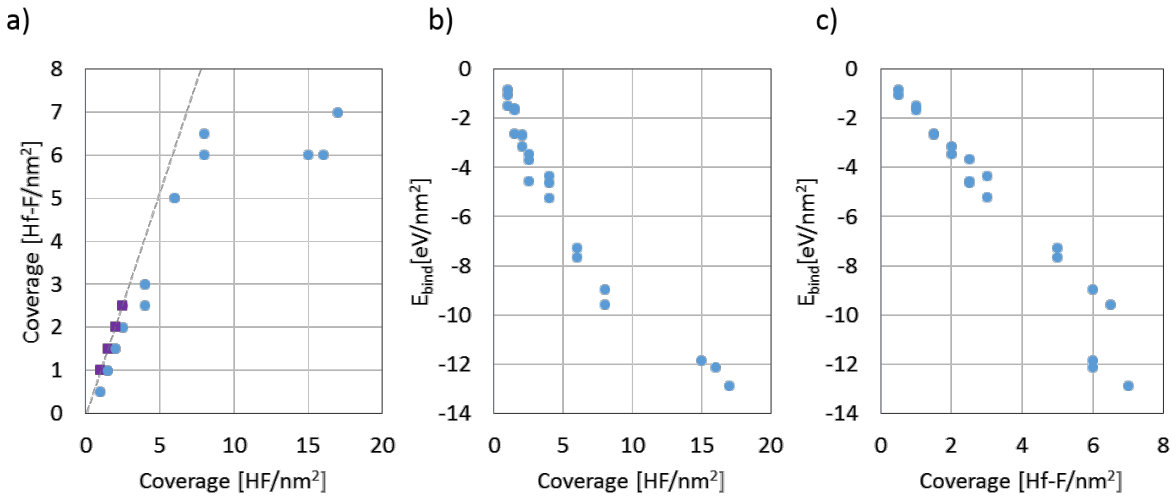

Figure 11: (a) Scatter plot for Hf-F coverage versus total HF coverage for the surface coverage values in Table 3. Note that some HF coverages resulted in partial or complete Hf-F coverage for different configurations for example the coverage of 1.0 HF/nm^2. The square data points are where the adsorbed HF coverage equals Hf-F coverage. The circular data points are where partially dissociated HF molecules are present. Plots b and c show the change in binding energy per square nanometer with an increase in HF and Hf-F coverage respectively.

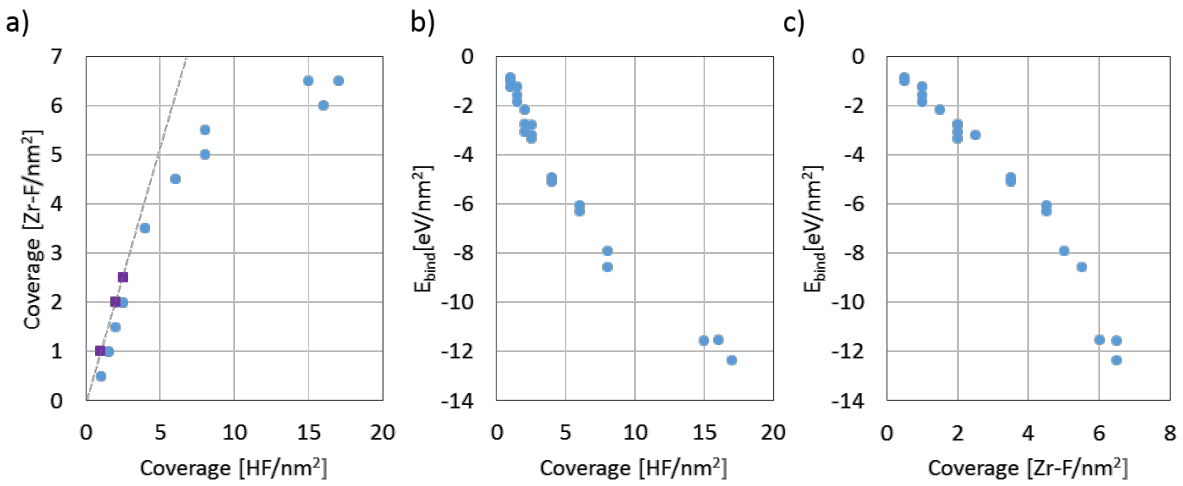

Figure 12: (a) Scatter plot for Zr-F coverage versus total HF coverage for the surface coverage values in Table 4. Note that some HF coverages resulted in partial or complete Zr-F coverage for different configurations for example the coverage of 1.0 HF/nm^2. The square data points are where the adsorbed HF coverage equals Zr-F coverage. The circular data points are where partially dissociated HF molecules are present. Plots b and c show the change in binding energy per square nanometer with an increase in HF and Zr-F coverage respectively.

Water Formation

The spontaneous formation of H_2O was observed in some of our relaxed geometries for the examples of 8C (3.0 ± 0.3 Hf-F/nm^2) on HfO_2 and 16A (5.0 ± 0.3 Zr-F/nm^2) on ZrO_2. The atomic structures are shown in Figure 13, where dissociation of at least two HF molecules provides the hydrogen atoms required to form H_2O as a reaction product, which removes oxygen from HfO_2, as discussed in,[9] but not discussed to date for ZrO_2. H_2O formation on the HfO_2 surface was observed on geometries 8HF C and 32HF, in which the H-O-H bond angle is 104.2 °. Similarly, H_2O formation on the ZrO_2 surface was observed on geometries 12HF B and 16HF A HF as shown in Figure 14. The H-O-H bond angle is 110.2 ° for 12HF B and for 16HF A 109.4 ° and 110.8°.

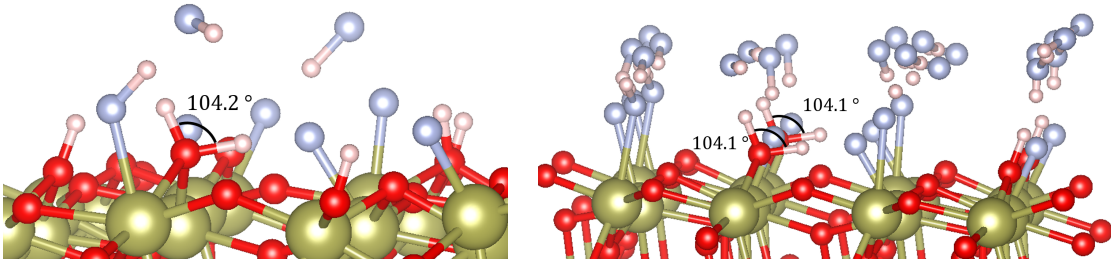

(a) Formation of 1 H_2O on HfO_2 8C HF (b) Formation of 2 H_2O on HfO_2 32 HF

Figure 13: Relaxed fluorination geometries for HfO_2 that resulted in H_2O forming spontaneously. Colour coding is the same as figure 8.

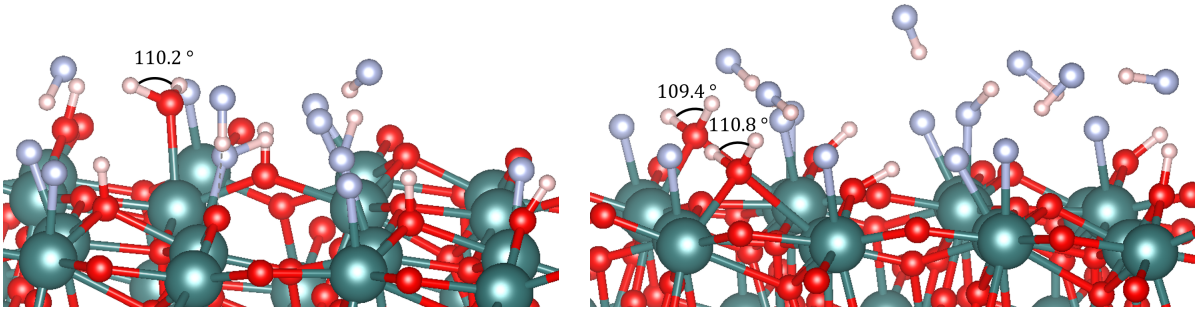

(a) Formation of 1 H_2O on ZrO_2 12B HF (b) Formation of 2 H_2O on ZrO_2 16A HF

Figure 14: Relaxed fluorination geometries for ZrO_2 that resulted in H_2O forming spontaneously. Colour coding is the same as figure 8.

The energy to remove H_2O (energy of desorption) from the fluorinated surfaces of 8HF C and 32HF for HfO_2 and 12HF B and 16HF A for ZrO_2 was calculated using equation 9,

$$E_{\text{des}} = (E\text{HfO}_{2(\text{surf})}/\text{HF}_{(\text{ads})} + E\text{H}_2\text{O}_{(\text{g})}) - (E\text{HfO}_{2(\text{surf})}/\text{HF}_{(\text{ads})}/\text{H}_2\text{O}_{(\text{ads})}.) \tag{9}$$

The term '$\text{EHfO}_{2(\text{surf})}/\text{HF}_{(\text{ads})}/\text{H}_2\text{O}_{(\text{ads})}$' is the total energy of HF adsorbed on HfO2 with spontaneous H2O formation. H_2O was removed from the fluorinated metal oxide surface with unbound HF molecules and the resulting geometry was relaxed. The term '$\text{EHfO}_{2(\text{surf})}/\text{HF}_{(\text{ads})}$' is the total energy of HF adsorbed on HfO2 after removing H2O from the surface and '$\text{EH}_2\text{O}_{(\text{g})}$' is the energy of gas phase H_2O molecule. The desorption energies of H_2O are presented in Table 5. These energies are relatively low and can be achievable at process conditions to remove surface bound H_2O.

Configuration	No. H_2O formed	$E_{(\text{des})}$ eV/H_2O
HfO_2		
8C HF	1	0.70
32 HF	2	1.32
ZrO_2		
12B HF	1	1.30
16A HF	2	0.50

Table 5: List of configurations that resulted in barrierless H_2O formation and the energy required to remove H_2O from their surface.

Discussion

From the N-E analysis, at all T $<$ 500 K using reactant and product pressures of 0.2 and 0.01 Torr respectively and a 8O:16F surface model as the SL product state, the HF pulse on HfO_2 and ZrO_2 is self-limiting in nature, as the reaction energies for the self-limiting reactions were more favourable than the spontaneous etching reactions. Therefore we suggest the first precursor pulse using HF, at these conditions, will produce a stable and nonvolatile layer of metal fluorides and H_2O as by products. We also found that at elevated temperatures,

the formation of the volatile metal fluoride is more favourable than the formation of the volatile metal oxyfluoride. The self-limiting nature of the fluorination reaction is due to the formation of a passivated layer during HF exposure.[26] The HfFx layer formed on HfO_2 after fluorination is self-limiting because this surface layer forms a diffusion barrier to subsequent fluorination by HF.[11] Multiple coverages of HF molecules starting from 1.0±0.3 to 17.0±0.3 HF/nm^2 resulted in mixed dissociated and molecular adsorption of HF to the surfaces of HfO_2 and ZrO_2. We found maximal coverages of 6.0±0.3 to 7.0±0.3 metal-F/nm^2 at higher HF coverages. Water forms spontaneously on relaxation from some of the geometries for multiple HF adsorption for both HfO_2 and ZrO_2. The computed desorption energies to remove H_2O from our fluorinated surfaces of HfO_2 and ZrO_2 are low enough to be overcome at process conditions.

For both HfO_2 and ZrO_2, the surfaces with an initial coverage of 17.0 ± 0.3 HF/nm^2 that resulted in 7.0 ± 0.3 Hf-F/nm^2 and 6.5 ± 0.3 Zr-F/nm^2 respectively are used to calculate a theoretical etch rate. Both (2x2) supercells of monoclinic (111) HfO_2 and ZrO_2 have surface areas of 1.98nm^2 with 16 metal atoms on the surface that can form metal-F bonds that correspond to a coverage of 8.0 ± 0.3 Hf/nm^2 and 8.0 ± 0.3 Zr/nm^2 respectively. As the maximum coverage of Hf-F is 7.0 ± 0.3 F/nm^2 there will be approximately 0.88 F atoms per surface Hf. The maximum coverage of Zr-F is 6.5 ± 0.3 F/nm^2, so there will be approximately 0.81 F atoms per surface Zr. The SE1 reactions showed that four F atoms lead to the etching of one Hf/Zr atom as volatile metal tetra-fluoride. Similar to the analysis done by Natarajan et al,[39] the coverage of Hf/Zr that can be etched is one quarter of the M-F coverage (M = Hf, Zr), 1.8 ± 0.1 Hf nm^{-2} cycle^{-1} for HfO_2 and 1.6 ± 0.1 Zr nm^{-2} cycle^{-1} for ZrO_2. As the surface concentration of metal atoms is 8.0 ± 0.3 Hf or Zr /nm^2 this etch rate corresponds to 0.2 monolayer/cycle. For HfO_2 this corresponds to -61.2 ± 0.8 ng cm^{-2} cycle^{-1} and using the mass density of bulk HfO_2 (10.0 g/cm^3), -0.61 ± 0.02 Å /cycle. For ZrO_2 this corresponds to -33.3 ± 0.8 ng cm^{-2} cycle^{-1} and using the mass density of bulk ZrO_2 (5.9 g/cm^3), -0.57 ± 0.02 Å /cycle. It is important to note that these computed etch rates do not take into

account kinetic effects that would be included in experimental etch rates. Therefore we also compute the maximum etch rate for the removal of a complete monolayer of material from HfO_2 and ZrO_2. We used 16 metal atoms for 1 ML removal which requires a Hf-F/Zr-F coverage of 32.32 ± 0.3 F/nm^2. An etch rate of -2.82 ± 0.02 Å /cycle was computed for 1 ML removal using the same method for calculating the theoretical etch rate. Therefore, if the etch rate is greater than -2.82 ± 0.02 Å /cycle, then it suggests that sub-surface metal atoms are being etched.

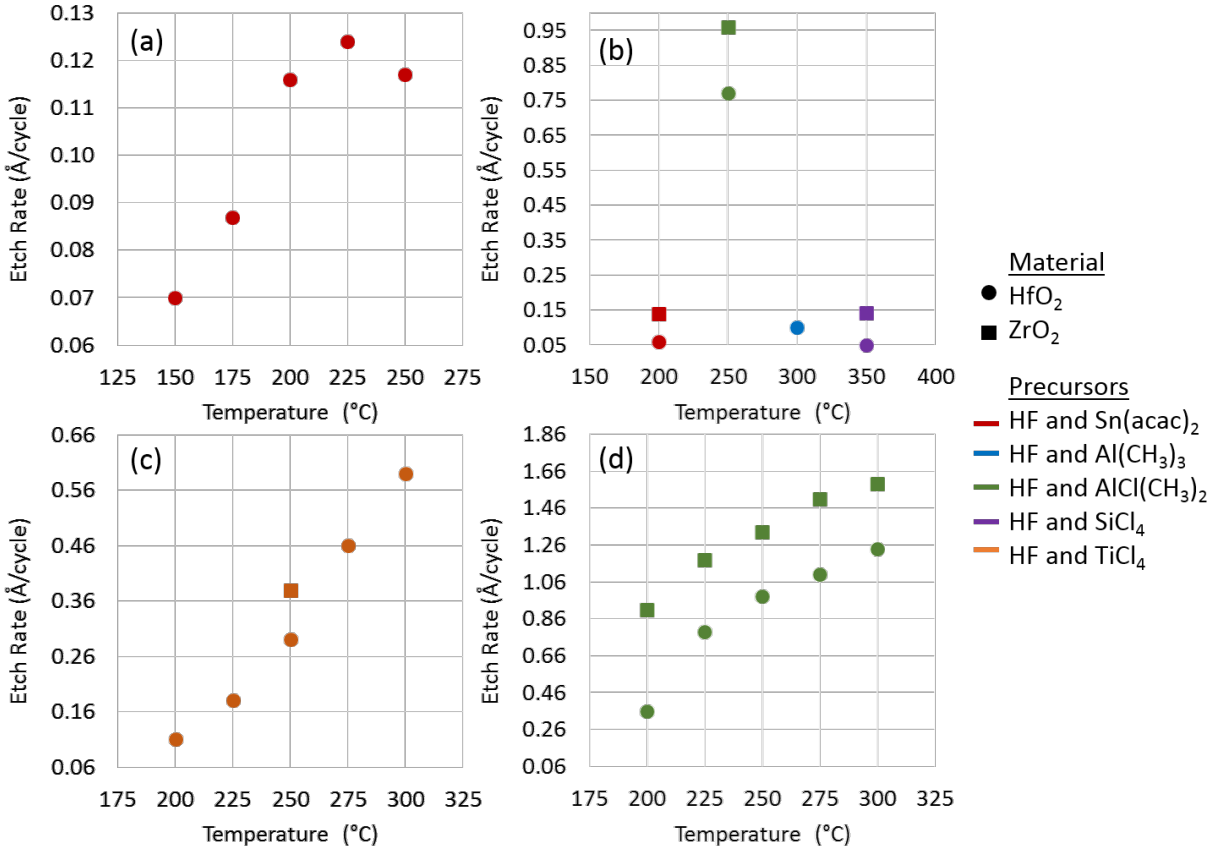

Figure 15: Experimental etch rates for the thermal ALE of HfO_2 and ZrO_2 using precursors HF and $Sn(acac)_2$,[4,9] $Al(CH_3)_3$,[4] $AlCl(CH_3)_2$,[4,12] $SiCl_4$[4] and $TiCl_4$.[11] Panel (a) shows the etch rates for the thermal ALE of HfO_2 using HF and $Sn(acac)_2$ for the temperature range 150-250 °C. Panel (b) shows the etch rates for the thermal ALE of HfO_2 and ZrO_2 using HF and $Sn(acac)_2$/ $AlCl(CH_3)_2$/ $Al(CH_3)_3$/ $SiCl_4$ at the temperatures shown. Panel (c) shows the etch rates for the thermal ALE using HF and $TiCl_4$ of HfO_2 for the temperature range 200-300 °C and ZrO_2 at 250 °C. Panel (d) shows the etch rates for the thermal ALE of HfO_2 and ZrO_2 using HF and $AlCl(CH_3)_2$ for the temperature range 200-300 °C.

A summary of experimental etch rates for HfO_2 and ZrO_2 using HF and a metal precursor

are shown in S5 of the Supporting Information and also in Figure 15. First thing we observe is that for a specific reactant combination, the etch rate increases with temperature for both materials and the etch rate for ZrO_2 is larger than that of HfO_2. We have predicted this from N-E analysis that the minimum barrier to continuous etch decreases considerably with an increase in temperature, more so in the case of ZrO_2 when compared to HfO_2. Between 150°C to 350 °C, for different reactant combinations, the etch rates can be anywhere between 0.05 Å /cycle and 1.24 Å /cycle for HfO_2 and between 0.01 Å /cycle to 1.59 Å /cycle for ZrO_2. The computed etch rate prediction given earlier based on the maximal M-F coverage (M = Hf, Zr) should be taken carefully as the experimental etch rate varies greatly with temperature and the reactant, in the second pulse. Moreover, the maximal experimental etch rate reported is much larger than the predicted etch rate suggesting that further reaction of adsorbed HF with the substrate is possible and this reaction surmounts the kinetic barriers which we have not included in this simple adsorption study. However, comparing the maximal etch rate of -2.82 ± 0.02 Å /cycle for 1 ML removal of Hf/ZrO_2 along with experimental etch rates, we can calculate the number of Hf/Zr removed per nm^2 in those experiments. Our surface model contains 8.0 ± 0.3 M/nm^2 (M = Hf, Zr) as mentioned earlier. So, an etch rate of -2.82 ± 0.02 Å /cycle correspond to a removal of 8.0 ± 0.3 M/nm^2 of the surface. Thus,

$$\text{No. of metal atoms removed per nm}^2 = \text{Expt. etch rate} \times -\frac{8.0}{2.8} \pm 0.1. \tag{10}$$

For example 4.5 ± 0.1 Zr atoms per nm^2 are removed as volatile ZrF_4 per cycle for an experimental etch rate of 1.59 Å /cycle using HF and DMAC at 300 °C. These results are also listed in S5 of the Supporting Information. It is clear that in all of these experiments, less than a monolayer of material is removed per ALE cycle. This computational approach detailed in this paper provides a general guideline to safely examine the influence of any reactant species on the substrate materials of interest.

Conclusion

We present DFT calculations to understand the nature of the HF pulse on the bare surfaces of monoclinic HfO_2 and ZrO_2 for thermal ALE. N-E analysis of the self-limiting and spontaneous (continuous) etching using simple reaction models representing the HF exposure on HfO_2 and ZrO_2 allowed us to predict if SL or SE reaction is favourable at a given T and at a given pressure, p. At $T < 500$ K, HF reaction with both oxides is found to be in the preferred self-limiting state. This is a relatively inexpensive way to screen the reactant molecules for ALE, also equally applicable to ALD, of any given substrate. We studied the adsorption of HF molecules on HfO_2 and ZrO_2 for HF coverages ranging from 1.0±0.3 - 17.0±0.3 HF/nm^2 along with analysis of H_2O formation. From this analysis, we predict a theoretical etch rate based on the maximum possible coverage of surface bound HF for HfO_2 and ZrO_2. The maximal computed metal-F coverage on both surfaces is from 6.0±0.3 to 7.0±0.3 metal-F/nm^2. The spontaneous formation of water was also seen at some HF coverages on both oxides. We calculated theoretical etch rates of -0.61 ± 0.02 Å /cycle for HfO_2 and -0.57 ± 0.02 Å /cycle for ZrO_2 which are lower than the maximal etch rates reported from experiments. The etch rate for a complete ML removal, -2.82 ± 0.02 Å /cycle, was used with experimental etch rates to compute the number of metal atoms removed from the surface per nm^2 per cycle. We can use the presented methodology for the first pulse on HfO_2 and ZrO_2 to examine other reagents such as HCl and HBr with a similar analysis as well as examining the interaction of HF on a hydroxyl terminated surfaces of HfO_2 and ZrO_2.

Acknowledgement

We acknowledge support for this work from LAM Research and from the Science Foundation Ireland-NSF China Partnership Program, NITRALD Grant number: 17/NSFC/5279. We are grateful for access to Tyndall computing facilities supported by SFI and the Irish Centre for High End Computing, www.ichec.ie

Supporting Information

The Supporting Information is available free of charge at `https://pubs.acs.org/doi/10.1021/acs.chemmaterXXXXXX`. Self-limiting surface models used for thermochemical analysis, binding sites of 1 HF molecule at HfO_2 and ZrO_2 in HF adsorption studies, summary of bond dissociation energies, mixed molecular and dissociative adsorption of HF molecules from HF adsorption studies, experimental etch rates of HfO_2 and ZrO_2 with the corresponding number of metal atoms removed per nm^2, addition energy from increasing HF coverages (PDF)

References

(1) Raghu, P.; Yim, C.; Shadman, F.; Shero, E. Susceptibility of SiO_2, ZrO_2, and HfO_2 dielectrics to moisture contamination. *AIChE Journal* **2004**, *50*, 1881 – 1888.

(2) Raghu, P.; Rana, N.; Yim, C.; Shero, E.; Shadman, F. Adsorption of Moisture and Organic Contaminants on Hafnium Oxide, Zirconium Oxide, and Silicon Oxide Gate Dielectrics. *J ELECTROCHEM SOC* **2003**, *150*.

(3) Hausmann, D. M.; Kim, E.; Becker, J.; Gordon, R. G. Atomic Layer Deposition of Hafnium and Zirconium Oxides Using Metal Amide Precursors. *Chem. Mater.* **2002**, *14*, 4350–4358.

(4) Lee, Y.; Huffman, C.; George, S. M. Selectivity in Thermal Atomic Layer Etching Using

Sequential, Self Limiting Fluorination and Ligand-Exchange Reactions. *Chem. Mater.* **2016**, *28*, 7657–7665.

(5) Oehrlein, G. S.; Metzler, D.; Li, C. Atomic Layer Etching at the Tipping Point: An Overview. *ECS J. Sol. State Sci. Technol.* **2015**, *4*, N5041.

(6) Kanarik, K. J.; Lill, T.; Hudson, E. A.; Sriraman, S.; Tan, S.; Marks, J.; Vahedi, V.; Gottscho, R. A. Overview of atomic layer etching in the semiconductor industry. *J. Vac. Sci. Technol. A* **2015**, *33*, 020802.

(7) George, S. M.; Lee, Y. Prospects for Thermal Atomic Layer Etching Using Sequential, Self-Limiting Fluorination and Ligand-Exchange Reactions. *ACS Nano* **2016**, *10*, 4889–4894.

(8) Yuan, G.; Wang, N.; Huang, S.; Liu, J. A brief overview of atomic layer deposition and etching in the semiconductor processing. 2016 17th International Conference on Electronic Packaging Technology (ICEPT). 2016; pp 1365–1368.

(9) Lee, Y.; DuMont, J. W.; George, S. M. Atomic Layer Etching of HfO_2 Using Sequential, Self-Limiting Thermal Reactions with $Sn(acac)_2$ and HF. *ECS J. Sol. State Sci. Technol.* **2015**, *4*, N5013.

(10) Lee, Y.; George, S. M. Atomic Layer Etching of Al_2O_3 Using Sequential, Self-Limiting Thermal Reactions with $Sn(acac)_2$ and Hydrogen Fluoride. *ACS Nano* **2015**, *9*, 2061–2070, PMID: 25604976.

(11) Lee, Y.; George, S. M. Thermal atomic layer etching of HfO_2 using HF for fluorination and $TiCl_4$ for ligand-exchange. *J. Vac. Sci. Technol. A* **2018**, *36*, 061504.

(12) Lee, Y.; George, S. M. Thermal Atomic Layer Etching of Al_2O_3, HfO_2, and ZrO_2 Using Sequential Hydrogen Fluoride and Dimethylaluminum Chloride Exposures. *J. Phys. Chem. C* **2019**, *123*, 18455–18466.

(13) DuMont, J. W.; Marquardt, A. E.; Cano, A. M.; George, S. M. Thermal Atomic Layer Etching of SiO_2 by a Conversion-Etch Mechanism Using Sequential Reactions of Trimethylaluminum and Hydrogen Fluoride. *ACS Appl. Mater. Interfaces* **2017**, *9*, 10296–10307, PMID: 28240864.

(14) Lee, Y.; DuMont, J. W.; George, S. M. Mechanism of Thermal Al_2O_3 Atomic Layer Etching Using Sequential Reactions with $Sn(acac)_2$ and HF. *Chem. Mater.* **2015**, *27*, 3648.

(15) Lee, Y.; George, S. M. Atomic Layer Etching of Al_2O_3 Using Sequential, Self-Limiting Thermal Reactions with $Sn(acac)_2$ and Hydrogen Fluoride. *ACS Nano* **2015**, *9*, 2061–2070.

(16) Lee, Y.; DuMont, J. W.; George, S. M. Trimethylaluminum as the Metal Precursor for the Atomic Layer Etching of Al_2O_3 Using Sequential, Self-Limiting Thermal Reactions. *Chem. Mater.* **2016**, *28*, 2994.

(17) Hennessy, J.; Moore, C. S.; Balasubramanian, K.; Jewell, A. D.; France, K.; Nikzad, S. Enhanced atomic layer etching of native aluminum oxide for ultraviolet optical applications. *J. Vac. Sci. Technol. A* **2017**, *35*, 041512.

(18) DuMont, J. W.; George, S. M. Competition between Al_2O_3 atomic layer etching and AlF_3 atomic layer deposition using sequential exposures of trimethylaluminum and hydrogen fluoride. *J. Chem. Phys.* **2017**, *146*, 052819.

(19) Johnson, N. R.; Sun, H.; Sharma, K.; George, S. M. Thermal atomic layer etching of crystalline aluminum nitride using sequential, self-limiting hydrogen fluoride and $Sn(acac)_2$ reactions and enhancement by H_2 and Ar plasmas. *J. Vac. Sci. Technol. A* **2016**, *34*, 050603.

(20) Lee, Y.; DuMont, J. W.; George, S. M. Atomic Layer Etching of AlF_3 Using Sequen-

tial, Self-Limiting Thermal Reactions with $Sn(acac)_2$ and Hydrogen Fluoride. *J. Phys. Chem. C* **2015**, *119*, 25385–25393.

(21) Lemaire, P. C.; Parsons, G. N. Thermal Selective Vapor Etching of TiO_2: Chemical Vapor Etching via WF_6 and Self-Limiting Atomic Layer Etching Using WF_6 and BCl_3. *Chem. Mater.* **2017**, *29*, 6653–6665.

(22) Lee, Y.; George, S. M. Thermal Atomic Layer Etching of Titanium Nitride Using Sequential, Self-Limiting Reactions: Oxidation to TiO_2 and Fluorination to Volatile TiF_4. *Chem. Mater.* **2017**, *29*, 8202–8210.

(23) Shinoda, K.; Miyoshi, N.; Kobayashi, H.; Izawa, M.; Ishikawa, K.; Hori, M. Rapid thermal-cyclic atomic-layer etching of titanium nitride in CHF_3/O_2 downstream plasma. *J. Phys. D: Appl. Phys.* **2019**, *52*, 475106.

(24) Xie, W.; Lemaire, P. C.; Parsons, G. N. Thermally Driven Self-Limiting Atomic Layer Etching of Metallic Tungsten Using WF_6 and O_2. *ACS Appl. Mater. Interfaces* **2018**, *10*, 9147–9154.

(25) Johnson, N. R.; George, S. M. WO_3 and W Thermal Atomic Layer Etching Using Conversion-Fluorination and Oxidation-Conversion-Fluorination Mechanisms. *ACS Appl. Mater. Interfaces* **2017**, *9*, 34435–34447, PMID: 28876892.

(26) Zywotko, D. R.; George, S. M. Thermal Atomic Layer Etching of ZnO by a Conversion-Etch Mechanism Using Sequential Exposures of Hydrogen Fluoride and Trimethylaluminum. *Chem. Mater.* **2017**, *29*, 1183–1191.

(27) Johnson, N. R.; Hite, J. K.; Mastro, M. A.; Eddy, C. R.; George, S. M. Thermal atomic layer etching of crystalline GaN using sequential exposures of XeF_2 and BCl_3. *Appl. Phys. Lett.* **2019**, *114*, 243103.

(28) Lim, W.; Park, J. B.; Park, J. Y.; Park, B. J.; Yeom, G. Y. Low damage atomic layer etching of ZrO_2 by using BCl_3 gas and ar neutral beam. *J. Nanosci.* **2009**, *9 12*, 7379–82.

(29) Dallorto, S.; Goodyear, A.; Cooke, M.; Szornel, J. E.; Ward, C.; Kastl, C.; Schwartzberg, A.; Rangelow, I. W.; Cabrini, S. Atomic layer etching of SiO_2 with Ar and CHF_3 plasmas: A self-limiting process for aspect ratio independent etching. *Plasma Process Polym.* **2019**, *16*, 1900051.

(30) Koh, K.; Kim, Y.; Kim, C.-K.; Chae, H. Quasi atomic layer etching of SiO_2 using plasma fluorination for surface cleaning. *J. Vac. Sci. Technol. A* **2018**, *36*, 01B106.

(31) Mameli, A.; Verheijen, M. A.; Mackus, A. J. M.; Kessels, W. M. M.; Roozeboom, F. Isotropic Atomic Layer Etching of ZnO Using Acetylacetone and O_2 Plasma. *ACS Appl. Mater. Interfaces* **2018**, *10*, 38588–38595.

(32) Ohba, T.; Yang, W.; Tan, S.; Kanarik, K.; Nojiri, K. Atomic layer etching of GaN and AlGaN using directional plasma-enhanced approach. *Jpn. J. Appl. Phys.* **2017**, *56*, 06HB06.

(33) Kauppinen, C.; Khan, S. A.; Sundqvist, J.; Suyatin, D. B.; Suihkonen, S.; Kauppinen, E. I.; Sopanen, M. Atomic layer etching of gallium nitride (0001). *J. Vac. Sci. Technol. A* **2017**, *35*, 060603.

(34) Miyoshi, N.; Kobayashi, H.; Shinoda, K.; Kurihara, M.; Watanabe, T.; Kouzuma, Y.; Yokogawa, K.; Sakai, S.; Izawa, M. Atomic layer etching of silicon nitride using infrared annealing for short desorption time of ammonium fluorosilicate. *Jpn. J. Appl. Phys.* **2017**, *56*, 06HB01.

(35) Lu, W.; Lee, Y.; Gertsch, J. C.; Murdzek, J. A.; Cavanagh, A. S.; Kong, L.; del Alamo, J. A.; George, S. M. In Situ Thermal Atomic Layer Etching for Sub-5 nm InGaAs Multigate MOSFETs. *Nano Letters* **2019**, *19*, 5159–5166, PMID: 31251069.

(36) Gertsch, J. C.; Cano, A. M.; Bright, V. M.; George, S. M. SF_4 as the Fluorination Reactant for Al_2O_3 and VO_2 Thermal Atomic Layer Etching. *Chem. Mater.* **2019**, *31*, 3624–3635.

(37) Rahman, R.; Mattson, E. C.; Klesko, J. P.; Dangerfield, A.; Rivillon-Amy, S.; Smith, D. C.; Hausmann, D.; Chabal, Y. J. Thermal Atomic Layer Etching of Silica and Alumina Thin Films Using Trimethylaluminum with Hydrogen Fluoride or Fluoroform. *ACS Appl. Mater. Interfaces* **2018**, *10*, 31784–31794, PMID: 30179460.

(38) Fang, C.; Cao, Y.; Wu, D.; Li, A. Thermal atomic layer etching: Mechanism, materials and prospects. *Prog. Nat. Sci. Mater.* **2018**, *28*, 667 – 675.

(39) Kondati Natarajan, S.; Elliott, S. D. Modeling the Chemical Mechanism of the Thermal Atomic Layer Etch of Aluminum Oxide: A Density Functional Theory Study of Reactions during HF Exposure. *Chem. Mater.* **2018**, *30*, 5912–5922.

(40) Kresse, G.; Furthmuller, J. Efficient iterative schemes for ab initio total-energy calculations using a plane-wave basis set. *Phys. Rev. B* **1996**, *54*, 11169.

(41) Perdew, J. P.; Burke, K.; Ernzerhof, M. Generalized gradient approximation made simple. *Phys. Rev. Lett.* **1996**, *77*, 3865.

(42) Kresse, G.; Joubert, D. From ultrasoft pseudopotentials to the projector augmented-wave method. *Phys. Rev. B* **1999**, *59*, 1758.

(43) Lowther, J. E.; Dewhurst, J. K.; Leger, J. M.; Haines, J. Relative stability of ZrO_2 and HfO_2 structural phases. *Phys. Rev. B* **1999**, *60*, 14485–14488.

(44) Zhao, X.; Vanderbilt, D. First-principles study of structural, vibrational, and lattice dielectric properties of hafnium oxide. *Phys. Rev. B* **2002**, *65*, 233106.

(45) Togo, A.; Tanaka, I. First principles phonon calculations in materials science. *Scr. Mater.* **2015**, *108*, 1–5.

(46) TURBOMOLE V6.2 2010, a development of University of Karlsruhe and Forschungszentrum Karlsruhe GmbH, 1989-2007, TURBOMOLE GmbH, since 2007; available from `http://www.turbomole.com` last accessed 27/11/2019.

(47) Schäfer, A.; Huber, C.; Ahlrichs, R. Fully optimized contracted Gaussian basis sets of triple zeta valence quality for atoms Li to Kr. *J. Chem. Phys.* **1994**, *100*, 5829–5835.

(48) Schäfer, A.; Horn, H.; Ahlrichs, R. Fully optimized contracted Gaussian basis sets for atoms Li to Kr. *J. Chem. Phys.* **1992**, *97*, 2571–2577.

(49) Luo, Y. R. *Comprehensive Handbook of Chemical Bond Energies*; CRC Press: Boca Raton, FL, 2007.

Graphical TOC Entry